Biochemistry (Moscow), Vol. 66, No. 2, 2001, pp. 211-220. Translated from Biokhimiya, Vol. 66, No. 2, 2001, pp. 261-272.
Original Russian Text Copyright © 2001 by Yakovlev, Shuvalov.

Charge Separation in Photosynthetic Reaction Centers under Femtosecond Excitation

A. G. Yakovlev[1] and V. A. Shuvalov[1,2]*

[1]*Belozersky Institute of Physico-Chemical Biology, Lomonosov Moscow State University, Moscow, 119899 Russia; fax: (095) 939-3181*
[2]*Institute of Basic Biological Problems, Russian Academy of Sciences, Pushchino, Moscow Region, 142292 Russia; fax: (277) 90532; E-mail: shuvalov@issp.serpukhov.su*

Received April 27, 2000
Revision received September 29, 2000

Abstract—The process of electron transfer from the primary electron donor P* to the primary electron acceptor B_A in the reaction center of *Rhodobacter sphaeroides* R-26 under 30 fsec pulse excitation was studied in this work with the aim of establishing a relationship between the nuclear subsystem motion and charge transfer. For this purpose the fsec and psec oscillations in the bands of stimulated emission of P* and in the band of reaction product B_A^- at 1020 nm were investigated. It was established that the reversible formation of the $P^+B_A^-$ state is characterized by two vibration modes (130 and 320 cm^{-1}) and connected with an arrival of the wavepacket induced by fsec excitation to the intersection of potential surfaces P^*B_A and $P^+B_A^-$. The irreversible formation of the $P^+B_A^-$ state with the time constant of 3 psec is followed by oscillations with frequencies of 9 and 33 cm^{-1}. These results show that the irreversibility of electron transfer is determined by two factors: 1) by a difference between the energy width of the wavepacket and the gap between the named surfaces; 2) by a difference between the duration of wavepacket residence near the intersection of the surfaces and the relaxation time of the $P^+B_A^-$ state.

Key words: photosynthesis, reaction center, electron transfer, wavepacket, femtosecond spectroscopy

The reaction center (RC) of purple bacteria consists of three protein subunits (L, M, and H for light, medium, and heavy, respectively), four bacteriochlorophyll molecules, two bacteriopheophytin molecules, two quinone molecules, and one non-heme iron atom. The complete 3-D structure of RC has been determined by X-ray analysis [1-4]. Two bacteriochlorophyll molecules form a dimer that is the primary electron donor, P. It is shifted to the side of the photosynthetic membrane that corresponds to the lumen surface of chloroplast membrane. P is located at the axis of C_2-symmetry of the RC. Bilaterally along this axis and deeper in the membrane are located two molecules of monomer bacteriochlorophyll (B_A and B_B, where indexes A and B denominate the photoactive (A) and non-photoactive (B) chain of chromophores), and then two bacteriopheophytin molecules (H_A and H_B). At the opposite side of the membrane corresponding to the stromal surface of the chloroplast membrane, terminal electron acceptors, quinones Q_A and Q_B, are located also bilaterally of the axis of C_2-symmetry of the RC. The electron transfer passes via chromophores of the active chain (P, B_A, H_A, and Q_A) with high efficiency (quantum yield of 100%) [3]. Then the electron from Q_A^- is transferred to Q_B via the Fe atom which is liganded by four histidine residues and is located at the axis of C_2-symmetry of the RC.

A large body of research [5-13] has established that the primary act of charge separation in reaction centers (RCs) of purple bacteria is electron transfer from the excited primary electron donor P* to a monomeric bacte-

Abbreviations: RC) reaction center; P) primary electron donor, a dimer of bacteriochlorophyll molecules; B_A) primary electron acceptor, the monomer bacteriochlorophyll molecule localized in the active chain; B_B) monomer bacteriochlorophyll localized in the non-active chain; H_A) the bacteriopheophytin localized in the active chain; Q_A) the quinone localized in the active chain; Pheo) a plant pheophytin; $\Psi(x,t)$) wavefunction; φ_{n+j}) fundamental harmonic oscillator function; ΔG^o) free energy; ΔA) absorption difference ("light minus dark"); k) rate constant of electron transfer; $\sigma(r)$) transmission coefficient; υ) frequency factor; ΔG^*) free energy of activation; E_{reor}) reorganization energy; V) electron interaction energy between P and B_A; P^o_{WP}) probability of transition of wavepacket to the potential surface of state $P^+B_A^-$; ΔE_{WP}) energy width of wave packet; E_{WP}) energy of wave packet; ΔV_{elec}) energy of electrostatic interaction; ΔV_{QQ}) interaction energy between P and B_A; $\Delta V_{Q\mu}$) interaction energy of P and B_A with protein and crystal water atoms; ΔV_{ind}) interaction energy of P and B_A with induced dipoles.

* To whom correspondence should be addressed.

riochlorophyll molecule B_A. This step occurs within ~3 psec at 293K. Then the electron is transferred from B_A^- to a bacteriopheophytin H_A within ~1 psec and from H_A^- to quinine Q_A within ~ 200 psec. Decreasing the temperature to 5-10 K accelerates all these processes 2-3-fold. The appearance of the P* state results in bleaching of P absorption bands at 870 and 600 nm and in a stimulated emission at 920 nm as well. In parallel with electron transfer from P* to B_A, the stimulated emission at 920 nm decreases and is accompanied by bleaching of a B_A absorption band at 800 nm and appearance of a B_A^- absorption band at 1020 nm. This process is more pronounced with RCs in which H_A is replaced by plant pheophytin (Pheo) [13] since the $Pheo^-$ redox potential value is more negative than that of H_A. The energy of P^+Pheo^- state is ~200 cm^{-1} above that of $P^+B_A^-$ [14]. As a result, electron transfer from B_A^- to Pheo is absent at low temperature. Pheo takes a virtual part in electron transfer from B_A^- to Q_A with time constant 1.8 nsec instead of 100 psec in native RCs at 5K [13].

The recombinant fluorescence method has shown [15, 16] that the energy of the $P^+B_A^-$ state is 350-550 cm^{-1} lower than the energy of P^*B_A. The recombination time of $P^+B_A^-$ is about 1 nsec [13], this being threefold lower than the P*B lifetime (≈300 psec). The electron transfer from B_A^- to H_A is followed by lose of a free energy portion from 0.12 eV [5] to 0.25 eV [17]. For RCs from *R. viridis*, it was recognized by measuring $E_{1/2}$ [18] that the free energy decrease (ΔG^o), due to the transition from P^*H_A to $P^+H_A^-$ state is about 0.07 eV or 570 cm^{-1}; this is equal to the ΔH value determined by the recombination fluorescence. For these RCs the values $E_{1/2}$ were directly determined for P/P^+ (+515 mV) and for H_A^-/H_A (−620 mV) [18]. The sum of these values give $\Delta G^o = 1.14$ eV, which is 0.06 eV lower than the energy of the light quantum of the 0–0 transition of P (1015 nm). A similar value (0.08 eV or 645 cm^{-1}) was determined for ΔH. Hence it follows that the $P^+B_A^-$ and $P^+H_A^-$ states may be quite close to each other in RCs of this type; this has been shown experimentally as well [19]. The recombination time of $P^+H_A^-$ is 15 nsec at 293K and 20 nsec at 77K [20]; this is 20-fold slower than the recombination time of $P^+B_A^-$ according to the distance between the centers of P and B_A (11 Å) and P and H_A (16 Å).

Thus the primary act of charge separation in bacterial RCs takes place with the participation of two species, P* and B_A. The process has a time constant of 1.6 psec at 5K (see [13]) and 3 psec at 293K (see [21]). Most simply, the $P^+B_A^-$ state is recorded at modified RCs in which the bacteriopheophytin molecule H_A is replaced by a plant pheophytin molecule Pheo. Thus, in this work the mechanism of the primary act was studied using modified RCs.

Femtosecond absorption spectroscopy of chemical and biological systems permits not only to determine the sequence of a reaction, by the electron transfer for example, but to follow the motion of the nuclear subsystem resulting from the electron transfer as well. Actually, when a chromophore (P in our case) is excited by very short (⩽30 fsec) pulses with broad spectral width the excited state, P*, is generated as a superposition of wavefunctions of many vibrations instead of one particular vibrational excitation and a so-called "wavepacket" is formed as follows (see, for example [22]):

$$\Psi(x,t) = (2\upsilon + 1)^{-0.5} \Sigma^j \varphi_{n+j} \exp\{-i\omega(n + j + 0.5)t\}, \quad (1)$$

where φ_{n+j} is the fundamental function of a harmonic oscillator and ω is the mechanical oscillation frequency. A remarkable property of the wavepacket (1) is that it looks like semi-classical particles.

Femtosecond oscillations in P* emission. When P is transferred from the ground to the excited state a wavepacket is formed which begins to move over the surface of potential free energy of the excited state P*. The wavepacket, being a superposition of nuclear wavefunctions, includes also the energy of excited electron, which varies along with the nuclear subsystem as well. As a result, the wavepacket has an emission whose spectrum is clearly time dependent because the surface of the P* state is shifted along the nuclear coordinate with respect to the ground state surface P (Fig. 1). It is evident from Fig. 1 that on excitation of P by femtosecond pulses (⩽30 fsec) the wavepacket is formed at the left side of the potential surface P*, being shifted to the right with respect to the surface of the ground state. Then motion of the wavepacket occurs on the surface with a 260 fsec period that was found in a number of works by Vos et al. [23-27]. When the wavepacket is at the left side of the surface, it emits fluorescence with wavelength near 895 nm, and when it is at the right side, then with wavelength near 930 nm. The difference of emission wavelengths depends on the distance between the emitting point at the P* surface and the point at the P surface connected by the vertical line. It is evident that the wavepacket spends most of the time in the region where its potential energy is minimal and kinetic energy is maximal. The points on the left and right sides of the surface of the wavepacket are visited once per period and in antiphase. In contrast, at the point where the wavepacket momentum is maximal (near the surface bottom) the wavepacket visits twice per period and spends minimal time at this point. Thus, the fluorescence of the wavepacket with apparent fsec antiphase oscillation is observed near 895 and 930 nm, where the formation of distinct emission peaks is recorded [21, 24]. Oscillations of emissions with different spectra and phases are possible only when a shift of the potential surfaces of the excited and ground states takes place. If such shift is absent, then the emission spectrum is time independent and the oscillations are absent too. For oscillations with 260-fsec period, a rapid decay is characteristic in native RCs. The second oscillation maximum at 930 nm is less than the first by a factor of 5 and is more than the third by a factor of 5

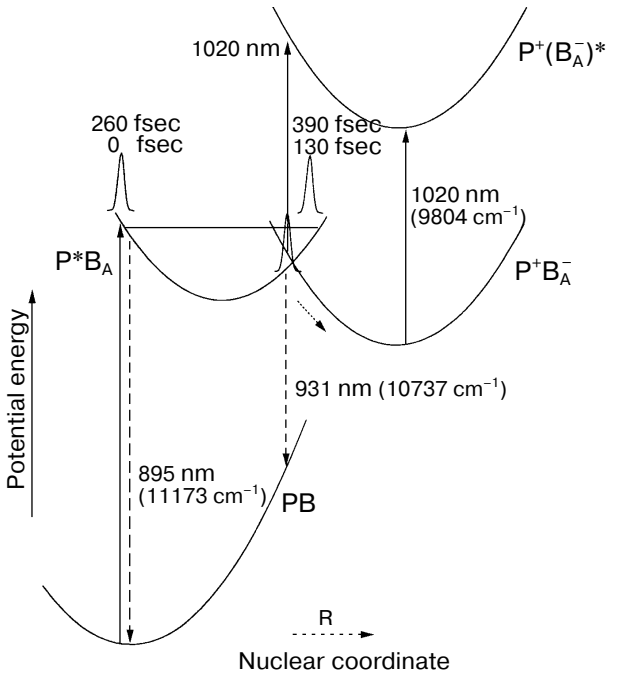

Fig. 1. Scheme of wavepacket motion along the potential surface of excited state P^*B_A and its emission from the opposite sides of the potential surface to the surface of the ground state PB_A. Intersection of potential surfaces P^*B_A and $P^+B_A^-$ at which the absorption band of B_A^- at 1020 nm has been observed is also shown. The same band is observed after thermalization of $P^+B_A^-$ because the shift of $P^+B_A^-$ and $P^+(B_A^-)^*$ surfaces is small.

too. Thus, only 20% of an initial wavepacket is able to enter the next cycle. In the D_{LL} mutant, oscillations with a changed period of 400 fsec are recorded near 945 nm and decay significantly slower: each subsequent maximum is 1.5-fold lower than the preceding one [23]. This fact points to a certain connection between the oscillations and the charge separation process.

Although so far the oscillations of only one mode were discussed, the whole spectrum of femtosecond oscillations of the stimulated emission of P*, which extends from 10 to 400 cm^{-1} and includes modes with frequencies at 15, 70, 92, 122, 153, 191, and 329 cm^{-1} [24], can be analyzed by means of Fourier transform. It is characteristic that the main part of the mentioned vibration modes was first found at 31, 73, 110, 147, 175, and 205 cm^{-1} [28] by the hole-burning method at 1.7K. Later, similar modes were found in Raman scattering spectra [29] at 34, 71, 95, and 128 cm^{-1}. Small difference between frequency values may be due to the used RCs isolated from different bacteria.

Femtosecond oscillations in the bands of the primary donor and acceptor of the electron in RCs. The charge separation between P* and B_A and the following electron transfer to H_A and Q_A occurs in bacterial RCs with 100% efficiency over a wide range of temperatures from 5 to 293K. Measurements of the electron transfer from P* to B_A with femtosecond time resolution are most interesting because just for that reaction it is possible to study the relationship of the nuclear wavepacket motion and the electron transfer. To study this question, measurements were carried out [30-32] in the P* stimulated emission band as well as in the B_A absorption band at 293K. Similar measurements were performed at 15K (see [33]), but in this case the contribution of P* in that spectral region is too high due to fine effects of B_A and B_B band shifts under the influence of P* and due to formation of bands characteristic of P*. As a result, it is difficult to see the oscillation connected with reduction of B_A. The situation is significantly easier at 293K because the B_A and B_B bands are broad and consequently the fine effects of band shifts under the field of P* are eliminated [30-32].

It was demonstrated [32] that on the short-wavelength side of the P* emission at 890 nm the period of initial intensive oscillations is located in the region of 240 fsec; that corresponds to an oscillation frequency of about 140 cm^{-1} which was recorded earlier in similar measurements at 10 K [24] as well as in the hole-burning spectra [28]. It is important also that this mode is the basis for P absorption simulation at different temperatures [34]. This means that one of the vibrational levels of this mode is populated when P is transferred to the excited state; that process leads to nuclear motions whose sense is discussed below.

As already mentioned, oscillations within the range 130-140 cm^{-1} are recorded also in the B_A absorption band at 805 nm in antiphase with the stimulated emission at 890 nm and, consequently, in phase with the emission at 930 nm [32]. Fourier transformation of the oscillation at 890 and 805 nm showed not only this mode but also another modes at 10, 32, 43, and 84 cm^{-1}. It is important that the amplitude ratio for some of these modes is different for 890 and 805 nm. The amplitude for the 130-140 cm^{-1} mode is practically the same, but the amplitude of oscillations at 10 and 32 cm^{-1} are significantly higher for the kinetics at 805 nm. The 32 cm^{-1} mode oscillations are clearly seen in the 2-3-psec part of the initial kinetics, this suggesting the real origin of this mode. As the absorption changes near 800 nm may reflect the changes in the B_A band, it was supposed [31, 32] that the oscillation at 130-140 and 32 cm^{-1} is directed along the reaction coordinate of electron transfer from P* to B_A. Both modes are clearly seen in the absorption spectrum of P [34] as well as in the hole-burning spectrum for P excitation in the 0–0 transition region [28]. This indicates the existence of remarkable amplitude of these oscillations under P excitation. This is also important for realization of their function in the electron transfer from P* to B_A. At the same time, it was noted [32] that a supplementary investigation on participation of these oscillations in the electron transfer is needed to make a final conclusion. This is due

to a possibility that these oscillations may be connected with the own oscillations of P*, with the B_A and B_B bands shift, and with absorption changes of B_A and B_B under the influence of the P* field. The two later possibilities as well as the possibility of oscillations due to the electron transfer from P* to B_A are not in contradiction with the fact that oscillations in the B band are in phase at both sides of the absorption at 800 nm [31, 32]. In contrast, the absorption of P* → P** or B → B* types for oscillations in P* state and in ground state B does not correspond to experimental data. Measurements [32] with the YM210W mutant having remarkably decreased rate of the electron transfer from P* to B_A showed that the 10 and 30 cm^{-1} modes are appreciably suppressed in the kinetics at 805 nm. This may indicate the participation of these modes in the charge separation process too. From another side, the molecular dynamics calculations [35] indicate the same possibility; these calculations show that the mode near 17 cm^{-1} modulates the distance between P and B_A. The change in the distance between P* and B_A may be important for the electron transfer.

At the same time, additional information about fsec oscillations in the product of charge separation $P^+B_A^-$ may significantly clarify this process. With this aim, measurement of the band formation at 1020 nm which belongs to the radical anion B_A^- and directly indicates the appearance of $P^+B_A^-$ was carried out in this work.

MATERIALS AND METHODS

RC of *Rhodobacter sphaeroides* R26 were isolated as described in [36]. The bacteriopheophytin was replaced by plant pheophytin according to the procedure described in [12]. The optical density of the samples was 0.5 at 860 nm at 293 K in a 1-mm cell. Dithionite (5 mM) addition to the samples with subsequent illumination by unfocused light of an incandescent lamp for ~1 min was used to maintain the $PB_AH_AQ_A^-$ state of the RCs. All measurements were carried out at room temperature.

A detailed description of the experimental setup constructed at the Belozersky Institute of Physico-Chemical Biology of Lomonosov Moscow State University can be found in [21]. A femtosecond mode-locked Ti:sapphire laser (26 fsec pulse duration) was used as the master generator of the spectrometer. A single pulse expanded to 10 psec by a stretcher was amplified by an 8-pass Ti:sapphire amplifier and then was compressed by a compressor to the initial fsec pulse width. The amplified fsec pulses were focused onto a water cell to produce a light continuum. An RG 850 filter (Melles Griot, USA) cut off the wavelength region below 850 nm. Approximately 96% of the total energy of the continuum was used for pump pulses and the remaining 4% for probe and reference pulses. The pump and probe pulses passed through a delay line and the sample. Then the probe and reference pulses were sent to a polychromator coupled to an optical multichannel analyzer (ORIEL, France). The operating frequency of the spectrometer was 2 Hz. The cross-correlation width of the pump and probe pulses corresponded to ~30 fsec pulse duration. The relative position of the zero time delay did not exceed 30 fsec within the 900-1100 nm region. The delay between pump and probe pulses was changed with an accuracy of ~20 fsec. The difference (light-minus-dark) absorption spectra $\Delta A(\lambda)$ are the results of averages of several hundred measurements.

RESULTS

Investigation of fsec oscillations in the B_A absorption band at 1020 nm was undertaken to solve the problem of the participation of definite oscillation modes in the charge separation in RCs. This band is sensitive to the formation of primary product, $P^+B_A^-$, i.e., of the charge separation between P* and B_A. This approach gives significant information about the mechanism of nuclear movement coupling in the P^*B_A state and the electron transfer

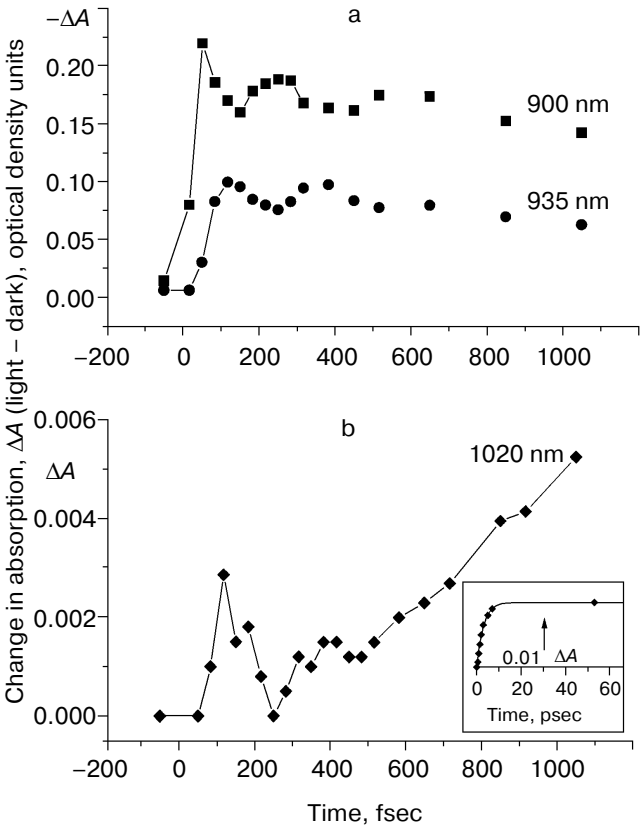

Fig. 2. Kinetics of ΔA at 900, 935, and 1020 nm for pheophytin-modified *Rb. sphaeroides* RCs excited by 30-fsec pulses at 870 nm at 293K. The inset shows the ΔA kinetics at 1020 nm from 0 to 53 psec.

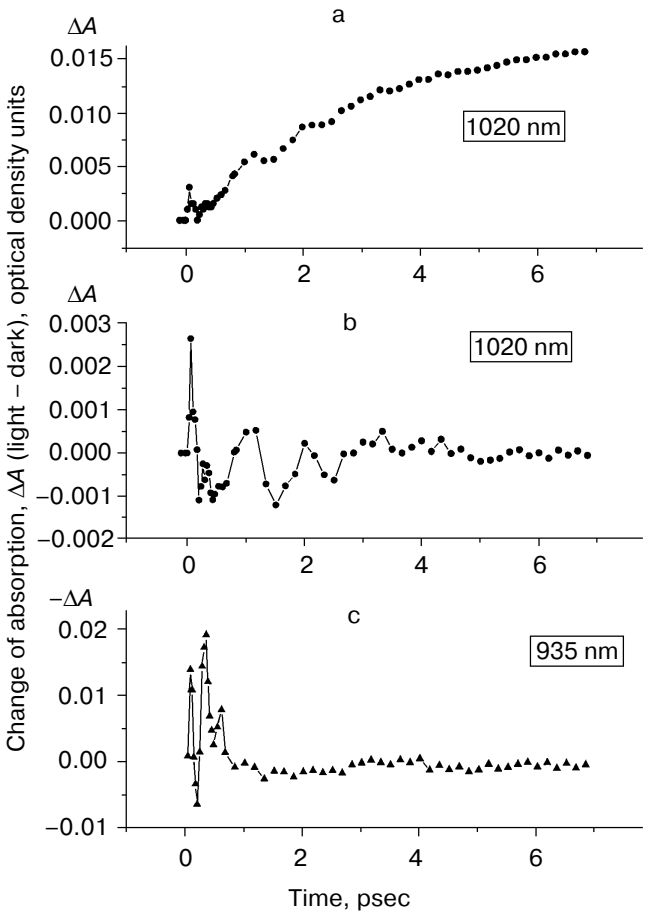

Fig. 3. Kinetics of ΔA at 1020 nm (a) and its oscillating part (b) and the oscillating part of ΔA kinetics at 935 nm (c) for pheophytin-modified *Rb. sphaeroides* RCs at 293K.

since the 1020-nm band is not present in the initial RC absorption. It is characteristic just for the radical anion of bacteriochlorophyll [37].

Figure 2 shows that the 1020-nm band formation in pheophytin-modified RCs from *Rb. sphaeroides* follows in phase oscillations of the P* stimulated emission at 935 nm (and it also follows in phase B_A band bleaching at 805 nm according to [32]). Appearance of the band at 1020 nm is reversible with ~120-fsec delay and partly reversible with 380-fsec delay as well as at 1 and 2 psec (Fig. 3). Characteristically, the in-phase oscillations at 935 and 1020 nm are out-of-phase with oscillations at 900 nm (the maximum at 895 nm [24]) (Fig. 2). Amplitudes of oscillations at 935 and 1020 nm for 120 fsec time delay normalized to the maximal ΔA values of these kinetics are close to each other (0.19 and 0.20, respectively). This means that to 120 fsec delay time a mixed state of P* and $P^+B_A^-$ is formed that emits light at 935 nm (P*) and absorbs at 1020 nm (B_A^-). The residence time of the wavepacket in the crossing region of two surfaces at 120 fsec delay is ~100 fsec.

The oscillation kinetics at 1020 nm, which is a difference of the initial kinetics (Fig. 3a) and exponentially increasing curve with 3 psec time constant, is shown in Fig. 3b. One can see an oscillation with ~1-psec period besides a fast oscillation with a ~260-fsec period. Such picosecond oscillations are not seen in the kinetic curve at 935 nm (Fig. 3c). Figure 4 shows results of a Fourier transformation of the oscillating part of the kinetics at 935 nm (a), 1020 nm (b), and 805 nm (c) (the latter is taken from [32]). All these spectra have a broad band with peak at 130-140 cm^{-1} (240-260 fsec period). At the same time, a characteristic frequency at 30-33 cm^{-1} (~1 psec period) that is seen in the Fourier spectra of kinetics at 805 and 1020 nm is lacking or significantly depressed in the Fourier spectrum of the kinetic curve at 935 nm. Modes at 27 and 42 cm^{-1} are observed in the 890-nm kinetics of native RCs, but their amplitudes are 2-3-fold lower than the amplitude of the 130-140 cm^{-1} mode [32]. The same relationship of these modes was observed in a hole-burning spectrum [28].

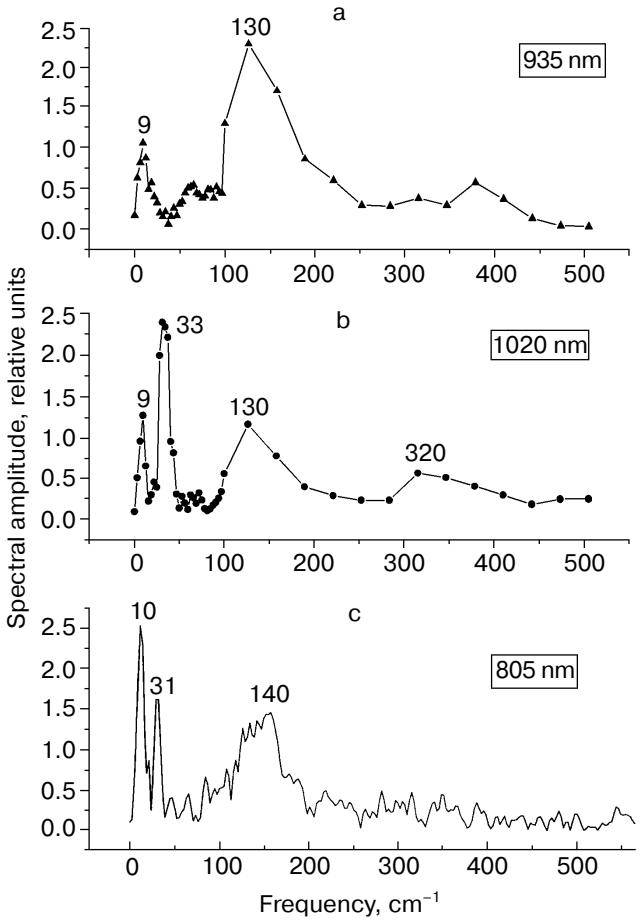

Fig. 4. Fourier transform spectrum of kinetics at 935 nm (a) and at 1020 nm (b) that are shown in Fig. 3 and of kinetics at 805 nm (c) from [32] for pheophytin-modified *Rb. sphaeroides* R-26 RCs.

The starting time of the 1-psec oscillations can be found by extrapolation of the periodic curve with peaks at 1, 2, and 3 psec to zero time (Fig. 3b). One can see that this start is at approximately the 100-fsec point of the time scale. Thus, it can be supposed that the 30-33 cm^{-1} mode is formed during the first approach of the wavepacket at the 130-140 cm^{-1} mode surface to an intersection with the $P^+B_A^-$ surface. The wavepacket lives about 600 fsec at the intersection of these two surfaces at 1 psec.

An enhancement of the 30-33 cm^{-1} mode in the Fourier spectrum of the appearing product $P^+B_A^-$ at 805 and 1020 nm indicates the fact that this mode reflects a motion of the nuclear subsystem along a reaction coordinate of the product $P^+B_A^-$. In contrast to the 130-140 cm^{-1} mode, which shows reversible electron transfer, the oscillation of the 30-33 cm^{-1} mode is accompanied by partially irreversible electron transfer (Figs. 2 and 3). Only ~50% of this transfer can be considered as reversible. These facts may be significant for the understanding of the mechanism of highly efficient charge separation in RCs.

DISCUSSION

Scheme of electron–vibration interactions of the charge separation in RCs. The theory of coupling of nuclear oscillations and electron transfer [38] forms the basis for the scheme (Fig. 5) summarizing the experimental data. In general, a rate constant of electron transfer, k, is determined by transmission coefficient $\sigma(r)$ showing the probability of the electron transfer from P* to B_A during one approach to the intersection area of the P^*B_A and $P^+B_A^-$ surfaces when r has a fixed value. This coefficient varies approximately as $\exp[-\beta(r - r_0)]$, where β is within 10-20 nm^{-1}, r_0 is equal to the distance for which $\sigma(r)\upsilon = 10^{13}$ sec^{-1}, and υ is a frequency factor. The expression for k also includes the exponential factor $\exp(-\Delta G^*/k_BT)$, where ΔG^* is a free activation energy:

$$k = \sigma(r)\upsilon \exp(-\Delta G^*/k_BT). \quad (2)$$

If significant electron coupling of two states (adiabatic reaction) takes place, then $\sigma(r)$ approaches 1. In this

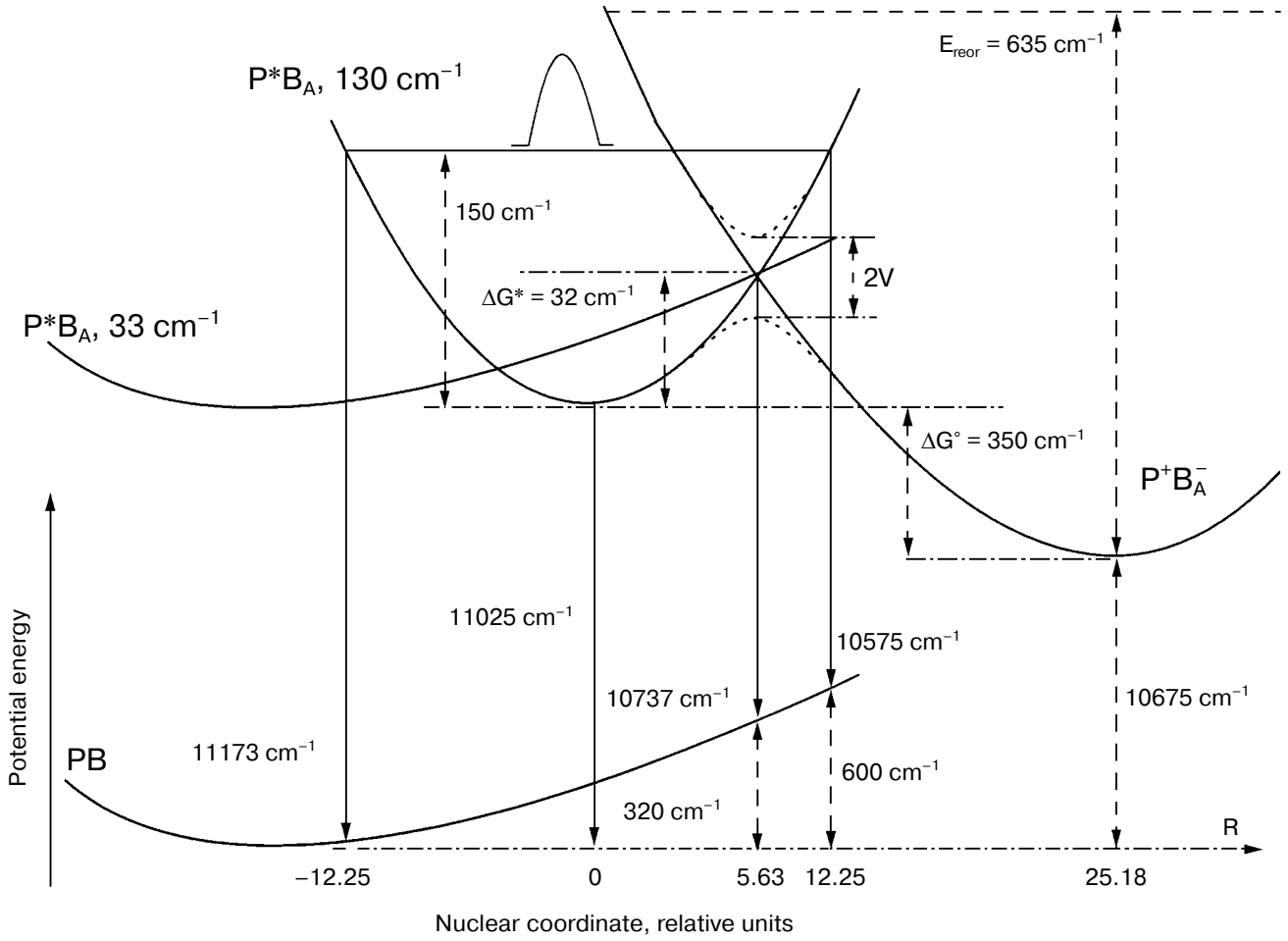

Fig. 5. Scheme of electron–vibration interactions of the charge separation in *Rb. sphaeroides* RCs. On the abscissa axis, values of the nuclear coordinate are plotted in relative units. On the ordinate axis, values of potential energy are plotted in cm^{-1}. In both cases an arbitrary scale was chosen for simplicity. See text for details.

case υ has the meaning of an effective frequency of the nuclear motion along the reaction coordinate. If σ(r) << 1 (non-adiabatic case), then the expression for *k* can be obtained according to quantum mechanical calculations. The constant of electron transfer rate (*k*) in the first approach is determined in the following way:

$$k = 2\pi/h\,|V|^2\,(4\pi E_{reor}\,k_B T)^{-0.5}\exp\{-$$
$$-(\Delta G^o + E_{reor})^2/(4E_{reor}\,k_B T)\}, \quad (3)$$

where E_{reor} is an energy of reorganization, ΔG^o is a free energy of reaction, and V is a coupling interaction value between P and B_A.

The results may indicate the necessity of modifying the assumed theory describing the relationship of the nuclear wavepacket motion and the electron transfer. Because the wavepacket represents a semi-classical particle (1) and the electron transfer occurs during each access to the intersection of the initial reagent surface (P^*B_A) and reaction product surface ($P^+B_A^-$) (an adiabatic reaction), then the classical approach (2) appears more appropriate for description of the process. However, it is seen from measurements of the mode with frequency 130-140 cm^{-1} that σ(r) has two independent components: 1) nuclear (nuc), and 2) electronic (el). Actually, practically complete mixing of states P* and $P^+B_A^-$ is observed at 120 fsec delay because the oscillation amplitudes at 930 and 1020 nm normalized to the maximal Δ*A* value at the corresponding wavelength are close to each other (0.19 and 0.2, respectively). This means that σ_{el} approaches 1. On the other hand, σ_{nuc} is equal to 0 because the electron transfer is fully reversible and the wavepacket as a whole returns to the P* state surface. That is why the transmission coefficient must be presented as a product of both named parts. Then Eq. (2) can be rewritten in the form:

$$k = \sigma_{nuc}\,\sigma_{el}\,\upsilon\exp(-\Delta G^*/k_B T). \quad (4)$$

In the case of the mode with 30-33 cm^{-1} frequency, σ_{el} is large as well due to the long residence of the wavepacket at the place of intersection. However, the σ_{nuc} value exceeds 0 because the electron transfer is irreversible in part (see below).

Figure 5 shows the ground state PB_A, the excited state P^*B_A, and the charge transfer state $P^+B_A^-$ presented as parabolic multidimensional surfaces of potential energy; in the figure these surfaces are shown by its parabolic cross-sections (one-dimensional curves). The potential curve of the P^*B_A state is shifted to the left along a nuclear coordinate R relative to the curve of PB_A. An absorption of P in RC has a maximum at 870 nm at 293K (890 nm at 10K) that corresponds to transfer at one of the vibration levels with the frequency of 130-140 cm^{-1} (see above). On excitation of P by femtosecond pulses (≤30 fsec), the wavepacket is formed at the specified surface and starts to move on the surface with 240-260 fsec period. Emission of the wavepacket at the left side of the potential curve (Fig. 5) corresponds to the short-wavelength emission at 895 nm (11,173 cm^{-1}) and at the right side to the long-wavelength emission at 931 nm (10,737 cm^{-1}). The maximum of the 0–0 transition is located near 907 nm (11,025 cm^{-1}) [34] and the emission maximum after a thermalization is at 920 nm (10,870 cm^{-1}). Considering this, it is possible to estimate that the initial potential energy of the wavepacket is 150 cm^{-1} above the energy of the bottom of the surface. Thus, the wavepacket for the 130-140 cm^{-1} mode may include a superposition of wavefunctions of three vibration levels 0, 1, and 2 if each level has approximately the same contribution.

An emission of the wavepacket at 931 nm (10,737 cm^{-1}) is asymmetric relative to the 0–0 transition (11,025 cm^{-1}) and to the emission at 895 nm (11,173 cm^{-1}). The symmetric emission is located at 946 nm (10,575 cm^{-1}) and was not observed experimentally. A possible explanation of this fact may be that the wavepacket emits at some point of a potential surface that is significantly distorted under some physical disturbances. An intersection with the potential surface of the reaction product $P^+B_A^-$ may serve as such disturbance (Fig. 5). This assumption is in accordance with presented experimental data.

The frequencies indicated in Fig. 5 show that the surface intersection point is at a level of 32 cm^{-1} from the bottom of P^*B_A. The scheme can be used to find the reorganization energy, E_{reor}, which is equal to 635 cm^{-1}. An independent determination of E_{reor} gave a value of 1.6 kcal/mol or 560 cm^{-1} [39], this being close to the value from obtained from the scheme in Fig. 5.

Since the value of electron coupling of P and B_A (V) is in the range from 6 to 32 cm^{-1} [40-42], this means that the intersection of the P^*B_A and $P^+B_A^-$ surfaces is split by a value of $2V \cong 30$ cm^{-1}. So the barrier between P^*B_A and $P^+B_A^-$ states does not exceed ~15 cm^{-1}.

As found, the point of intersection of the surfaces is at 32 cm^{-1} above the bottom of the P^*B_A surface. This may indicate also that the wavepacket meets an obstacle in a form of splitting surfaces at the surface of the 130-140 cm^{-1} mode, resulting in its dephasing. If another mode surface (about 30 cm^{-1}) is nearby, then the wavepacket may pass to the new surface, losing some part of its energy. The period of the wavepacket oscillation increases to 1 psec in this case. The duration of wavepacket residence near the intersection increases too. This assumption is proved by the experimental data. Actually, the time of appearance of the 33 cm^{-1} oscillation coincides with the time of the first peak at 1020 nm at 120 fsec (130 cm^{-1} mode), i.e., at the P^*B_A and $P^+B_A^-$ intersection point (Figs. 2 and 3). From the other side, Fourier transform of oscillations at 10K [24] contains several modes at 31, 69, 92, 122, and 153 cm^{-1} on the background of the broad band near 130 cm^{-1}. On average, frequencies of these modes are different at 31 cm^{-1}. This 31 cm^{-1} frequency may be a fundamental one, while all other may be its harmonics. In other words,

the wavepacket with 130-140 cm^{-1} frequency can be split into harmonics of the 30-33 cm^{-1} mode in the vicinity of the P* and $P^+B_A^-$ surfaces intersection point. If the duration of wavepacket residence near the intersection point for the 130-140 cm^{-1} mode at 120 fsec is ~100 fsec, then for the 30-33 cm^{-1} mode at 1 psec this time increases to ~600 fsec (Fig. 3).

The scheme in Fig. 5 also explains the difference in oscillation amplitudes of the 130-140 and 30-33 cm^{-1} modes observed on the P^*B_A surface and in the $P^+B_A^-$ product. The 30-33 cm^{-1} mode may have minor amplitude under direct P excitation, unlike the 130-140 cm^{-1} mode, which determines the absorption spectrum of P and whose vibration levels accept the excited electron [34]. However when the wavepacket reaches the intersection of the P^*B_A and $P^+B_A^-$ surfaces at the level of 32 cm^{-1} above the P^*B_A surface bottom, the wavepacket motion of the 130-140 cm^{-1} mode suffers dephasing and passing to the 30-33 cm^{-1} mode surface. This is clearly seen in the product wavelength at 1020 nm.

The reversibility and probability of the electron transfer at the intersection point of the P^*B_A and $P^+B_A^-$ surfaces is determined by at least two factors. The first is related to the energy width of the wavepacket ($\geqslant$300 cm^{-1}) on the 130-140 cm^{-1} mode surface that is too large in comparison with the energy gap between the surfaces ($2V \cong$ 30 cm^{-1}). As a result, the probability of the wavepacket transition (P^o_{wp}) to the potential surface of $P^+B_A^-$ state does not exceed 0.1. After reaching the intersection point, the wavepacket returns back to the same P^*B_A surface with the 130-140 cm^{-1} frequency or to the 30-33 cm^{-1} surface. During the wavepacket motion on the surface of 30-33 cm^{-1} frequency, its width probably does not exceed 60 cm^{-1} and is comparable with the energy gap between the surfaces ($\cong$30 cm^{-1}). That is why the first factor is not absolutely limiting for the passage of the wavepacket to the $P^+B_A^-$ state surface.

The second factor is connected with a relationship between the rate of electron transfer at the intersection point of surfaces and the duration of wavepacket residence at this point. This relation can be estimated by comparison of initial oscillation amplitudes normalized to the maximal amplitude ΔA at 935 nm (relative amplitude of the wavepacket at the P* surface) and at 1020 nm (relative amplitude of the wavepacket at the $P^+B_A^-$ surface). According to Figs. 2 and 3, at 120-fsec time delay this ratio is equal to 0.19/0.20, respectively. This means that almost all electron density distributes between P* and B_A when the wavepacket is near the intersection point at this time delay.

In contrast, the duration of wavepacket residence near 1-psec delay (Fig. 3b) for the 33 cm^{-1} mode is about 600 fsec. The electron can be distributed between P* and B_A even more effectively. Reversibility of this transfer is determined most probably by an ability of the wavepacket transition from one surface (P^*B_A) to another ($P^+B_A^-$). As mentioned above, the energy widths of the wavepacket for this mode (about 60 cm^{-1}) exceeds twofold or less the energy gap (about 30 cm^{-1}) between the surfaces. Therefore, $\geqslant$50% of RCs may be transferred to the $P^+B_A^-$ state irreversibly. Figure 3a shows that the reversibility of the electron transfer is about 50% within the interval from 0.5 to 1.5 psec, in line with the above estimates.

The question of what is a driving force of the wavepacket transition from one surface to another is interesting too. Previously, we denoted P^o_{wp} as the probability for the wavepacket to pass through the point of intersection of the two surfaces:

$$P^o_{WP} \cong 2V/\Delta E_{WP}, \quad (5)$$

where ΔE_{wp} is the energy width of the wavepacket and 2V is the width of the gap between the surfaces.

However, the full probability must include an exponential factor if the wavepacket energy, E_{wp}, is less than the energy barrier at the intersection point of the two surfaces (ΔG^* in Fig. 5). Thus, it is necessary to use an additional factor ($\exp[-\Delta G^*/E_{wp}]$):

$$P_{wp} = 2V/\Delta E_{wp} \exp(-\Delta G^*/E_{wp}). \quad (6)$$

From (6) it follows that if $E_{wp} >> \Delta G^*$, then $P_{wp} = P^o_{wp}$. This suggests that the wavepacket kinetic energy must be positive at the place of potential surface intersection for the free wavepacket motion from one surface to another. When $E_{wp} = \Delta G^*$ (kinetic energy is equal to 0), the factor $\exp(-\Delta G^*/E_{wp}) = 0.368$ is almost 3-fold lower than 1.

It is evident from Fig. 5 that ΔG^* does not exceed 15 cm^{-1} when the surface splitting is taken into account. Thus, the factor $\exp(-\Delta G^*/E_{wp}) = 0.68$ for the 33 cm^{-1} mode for which we assume $E_{wp} \cong 30$ cm^{-1}. However, the real energy barrier may be less than 15 cm^{-1}. It follows also that the dimer nature of P may be important for the creation of the initial momentum of nuclear motion during the transition to the excited state that is necessary for effective electron transfer.

Of prime importance are the molecular dynamics calculations on the problem of the participation of certain oscillations of the nuclear subsystem in the electron transfer reaction. The question of certain oscillations of molecular groups participating in the electron transfer can be solved only by means of such calculations. One example of such calculation for *R. viridis* RCs is described in [35]. A sphere with 29-Å radius surrounded the center on the line between P and B. The electrostatic interaction energy ($\Delta V_{elec}(t)$) including interaction of P and B_A with each other (ΔV_{QQ}), with protein atoms and crystallographic water ($\Delta V_{Q\mu}$), with induced dipoles in protein and crystallographic water (ΔV_{ind}) was calculated. The molecular dynamic trajectories had a 1-fsec step at 293K, and $\Delta V_{elec}(t)$ values worked out after each 10 steps. An autocorrelation function $\Delta V_{elec}(t)$ of the PB_A and $P^+B_A^-$ states

was found from motion trajectories of these states. It was found that the autocorrelation function of the PB_A state oscillates with a frequency about 0.5 $psec^{-1}$ (17 cm^{-1}). These oscillations are suppressed in the $P^+B_A^-$ state. Also, it was found that the 17 cm^{-1} mode includes protein motions that modulate the relative position and orientation of the P and B_A molecules because the same frequency is observed in the autocorrelation function ΔV_{QQ} showing a direct interaction of primary electron donor and acceptor. It is important that the intense frequency at 28 cm^{-1} in ΔV_{QQ} was found in experiments on femtosecond oscillations.

Thus, the molecular dynamics calculations and fsec oscillations experiments show similar effects connected with mutual motions of P and B molecules that is also connected with the motions of some amino acid residues. First of all, this is related to the 30 cm^{-1} range of frequencies which accompany the irreversible charge separation in RCs as the experiment shows. In this connection, femtosecond investigations show that the excitation of a single electron of P does not result in charge separation. Only the motion of the nuclear subsystem, first in P* itself (probably with a frequency within the 130-140 cm^{-1} range) and then also in its environment including the B_A molecule as well leads finally to the electron transfer from P* to B_A with the creation of the primary product $P^+B_A^-$. This nuclear motion probably results in the shortest possible distance between P* and B_A or, in terms of the previous discussion, the movement takes place along the reaction coordinate up to the intersection point of the two potential surfaces of P^*B_A and $P^+B_A^-$. Momentum resulting from such motion can be used for the electron transfer when P* and B_A touch each other as well as for the further movement leading to a separation of reaction products P^+ and B_A^-. In other words, the coupled motion of nuclear and electron subsystems is a necessary condition for effective light energy conversion to the energy of separated charges in photosynthesis.

We thank Dr. A. V. Sharkov for his help during the femtosecond spectrometer construction and to Dr. A. Ya. Shkuropatov and Dr. V. A. Shkuropatova for RC isolation and modification. This work was supported by grants from the government of The Netherlands (NWO), INTAS, the Russian Foundation for Basic Research (grant No. 99-04-49120), and the "Universities of Russia–Fundamental Investigations" program.

REFERENCES

1. Deisenhofer, J., Epp, O., Miki, K., Huber, R., and Michel, H. (1985) *Nature*, **318**, 618-624.
2. Komiya, H., Yeates, T. O., Rees, D. C., Allen, J. P., and Feher, G. (1988) *Proc. Natl. Acad. Sci. USA*, **85**, 9012-9016.
3. Deisenhofer, J., Epp, O., Miki, K., Huber, R., and Michel, H. (1984) *J. Mol. Biol.*, **180**, 385-398.
4. Michel, H., Epp, O., and Deisenhofer, J. (1986) *The EMBO J.*, **5**, 2445-2451.
5. Shuvalov, V. A., and Klimov, V. V. (1976) *Biochim. Biophys. Acta*, **440**, 587-599.
6. Shuvalov, V. A., Klevanik, A. V., Sharkov, A. V., Matveetz, Yu. A., and Krukov, P. G. (1978) *FEBS Lett.*, **91**, 135-139.
7. Shuvalov, V. A., and Duysens, L. N. M. (1986) *Proc. Natl. Acad. Sci. USA*, **83**, 1690-1694.
8. Arlt, T., Schmidt, S., Kaiser, W., Lanterwasser, C., Meyer, M., Scheer, H., and Zinth, W. (1993) *Proc. Natl. Acad. Sci. USA*, **90**, 11757-11761.
9. Chekalin, S. V., Matveetz, Yu. A., Shkuropatov, A. Ya., Shuvalov, V. A., and Yartzev, A. P. (1987) *FEBS Lett.*, **216**, 245-248.
10. Schmidt, S., Arlt, T., Hamm, P., Huber, H., Nagele, T., Wachtveitl, J., Meyer, M., Scheer, H., and Zinth, W. (1994) *Chem. Phys. Lett.*, **223**, 116-120.
11. Schmidt, S., Arlt, T., Hamm, P., Huber, H., Nagele, T., Wachtveitl, J., Zinth, W., Meyer, M., and Scheer, H. (1995) *Spectrochim. Acta. Pt. A*, **51**, 1565-1578.
12. Shkuropatov, A. Ya., and Shuvalov, V. A. (1993) *FEBS Lett.*, **322**, 168-172.
13. Kennis, J. T. M., Shkuropatov, A. Ya., Stokkum, I. H. M., Gast, P., Hoff, A. J., Shuvalov, V. A., and Aartsma, T. J. (1997) *Biochem.*, **36**, 16231-16238.
14. Franken, E. M., Shkuropatov, A. Ya., Franke, C., Neerken, S., Gast, P., Shuvalov, V. A., Hoff, A. J., and Aartsma, T. J. (1997) *Biochim. Biophys. Acta*, **1321**, 1-9.
15. Shuvalov, V. A., and Yakovlev, A. G. (1998) *Biol. Membr. (Moscow)*, **15**, 455-460.
16. Nowak, F. R., Kennis, J. T. M., Franken, E. M., Shkuropatov, A. Ya., Yakovlev, A. G., Gast, P., Hoff, A. J., Aartsma, T. J., and Shuvalov, V. A. (1998) *Proc. XI Int. Congr. on Photosynthesis*, Kluwer Academic Publishers, Dordrecht, pp. 783-786.
17. Schenck, C. C., Blankenship, R. E., and Parson, W. W. (1982) *Biochim. Biophys. Acta*, **680**, 44-59.
18. Klimov, V. V., Shuvalov, V. A., Krakhmaleva, I. N., Klevanik, A. V., and Krasnovsky, A. A. (1977) *Biokhimiya*, **42**, 519-530.
19. Shuvalov, V. A., Amesz, J., and Duysens, L. N. M. (1986) *Biochim. Biophys. Acta*, **851**, 327-330.
20. Shuvalov, V. A., and Parson, W. W. (1981) *Proc. Natl. Acad. Sci. USA*, **78**, 957-961.
21. Yakovlev, A. G., Shkuropatov, A. Ya., and Shuvalov, V. A. (2000) *FEBS Lett.*, **466**, 209-212.
22. Sokolov, A. A., Loskutov, Yu. M., and Ternov, I. M. (1962) *Quantum Mechanics* [in Russian], Gos. Ucheb.-Pedagog. Izd-vo, Ministry of Education of Russian Federation, Moscow.
23. Vos, M., Rappaport, F., Lambry, J.-C., Breton, J., and Martin, J.-L. (1993) *Nature*, **363**, 320-325.
24. Vos, M., Jones, M. R., Hunter, C. N., Breton, J., Lambry, J.-C., and Martin, J.-L. (1994) *Biochemistry*, **33**, 6750-6757.
25. Vos, M. H., Jones, M. R., McGlynn, P., Hunter, C. N., Breton, J., and Martin, J.-L. (1994) *Biochim. Biophys. Acta*, **1186**, 117-122.
26. Vos, M. H., Jones, M. R., Hunter, C. N., Breton, J., and Martin, J.-L. (1994) *Proc. Natl. Acad. Sci. USA*, **91**, 12701-12705.
27. Vos, M. H., Jones, M. R., Breton, J., Lambry, J.-C., and Martin, J.-L. (1996) *Biochemistry*, **35**, 2687-2692.

28. Shuvalov, V. A., Klevanik, A. V., Ganago, A. O., Shkuropatov, A. Ya., and Gubanov, V. S. (1988) *FEBS Lett.*, **237**, 57-60.
29. Cherepy, N. J., Shreve, A. P., Moore, L. J., Franzen, S., Boxer, S. G., and Mathies, R. A. (1994) *J. Phys. Chem.*, **98**, 6023-6029.
30. Streltsov, A. M., Yakovlev, A. G., Shkuropatov, A. Ya., and Shuvalov, V. A. (1996) *FEBS Lett.*, **383**, 129-132.
31. Streltsov, A. M., Aartsma, T. J., Hoff, A. J., and Shuvalov, V. A. (1997) *Chem. Phys. Lett.*, **266**, 347-352.
32. Streltsov, A. M., Vulto, S. I. E., Shkuropatov, A. Ya., Hoff, A. J., Aartsma, T. J., and Shuvalov, V. A. (1998) *J. Phys. Chem. B*, **102**, 7293-7298.
33. Vos, M. H., and Martin, J.-L. (1999) *Biochim. Biophys. Acta*, **1411**, 1-20.
34. Klevanik, A. V., Ganago, A. O., Shkuropatov, A. Ya., and Shuvalov, V. A. (1988) *FEBS Lett.*, **237**, 61-64.
35. Parson, W. W., Chu, Z. T., and Warshel, A. (1998) *Photosynth. Res.*, **55**, 147-152.
36. Shuvalov, V. A., Shkuropatov, A. Ya., Kulakova, S. M., Ismailov, M. A., and Shkuropatova, V. A. (1986) *Biochim. Biophys. Acta*, **849**, 337-348.
37. Fajer, J., Brune, D. C., Davis, S., Forman, A., and Spanlding, L. D. (1975) *Proc. Natl. Acad. Sci. USA*, **72**, 4956-4960.
38. Marcus, R. A., and Sutin, N. (1985) *Biochim. Biophys. Acta*, **811**, 265-322.
39. Parson, W. W., Chu, Z. T., and Warshel, A. (1998) *Biophys. J.*, **74**, 182-191.
40. Parson, W., Warshel, A., Creighton, S., and Norris, J. (1988) in *The Photosynthetic Bacterial Reaction Center. Structure and Dynamics* (Breton, J., and Vermeglio, A., eds.) Plenum Press, N. Y., pp. 309-317.
41. Marcus, R. A. (1988) in *The Photosynthetic Bacterial Reaction Center. Structure and Dynamics* (Breton, J., and Vermeglio, A., eds.) Plenum Press, N. Y., pp. 389-398.
42. Zhang, L. Y., and Friesner, R. A. (1998) *Proc. Natl. Acad. Sci. USA*, **95**, 13603-13605.